

**Fluid flow in low aspect-ratio curved channels: from small to moderate Dean numbers.**

Ezzahrae Jaafari,<sup>1</sup> Pascale Magaud,<sup>2</sup> and Micheline Abbas<sup>1</sup>

<sup>1</sup>*Laboratoire de Génie Chimique, Université de Toulouse,  
CNRS, INPT, UPS, Toulouse, France*

<sup>2</sup>*Institut Clément Ader (ICA), Université de Toulouse CNRS,  
INSA, ISAE-SUPAERO, IMT Mines-Albi, Toulouse, France*

## Abstract

We investigated the pressure-driven flow in curved channels at low aspect ratio, the latter being the ratio between the channel height (along the axial direction) and width (along the radial direction). The dynamics was studied numerically, as a function of the characteristic Dean number,  $De = Re\sqrt{\delta}$ , by varying independently the Reynolds number  $Re$  and the curvature ratio  $\delta$ , the ratio between the hydraulic diameter and the radius of curvature. We considered the flow within a wide range of dimensionless numbers:  $De \lesssim 200$  and  $0.005 \leq \delta \leq 0.15$ . For  $De \lesssim 100$ , the flow remained stable in time, whereas at larger Dean numbers, the flow was stable while traveling several turns before transient structures developed. While investigating the flow features in the stable regime, only one pair of counter-rotating vortices was observed. At small  $De$  and large  $\delta$ , the peak of the streamwise velocity and the center of the vortices were located near the inner channel wall. They both shifted toward the outer wall as  $De$  was increased and/or  $\delta$  was decreased. This phenomenon is expected to have considerable impact on the interpretation of the transport of dispersed phase in multiphase flows in curved channels. Based on a dimensional analysis, the primary and secondary flow profiles, the friction coefficient of the flow as well as the flow development angle were all rationalized in terms of both  $Re$  and  $\delta$ .

## I. INTRODUCTION

The flow in a curved channel is of interest for particle sorting applications, among others, as the interplay between flow inertia at the particle scale and curvature effects promotes efficient particle focusing [1]. Recent studies suggest that using channels at low aspect ratio allows to enhance particle focusing with relatively short establishment lengths [2]. In this work, we consider particularly the flow in a curved rectangular channel with aspect ratio  $\lambda = 0.17$ , where  $\lambda$  denotes the ratio of the height (in the axial direction) and the width (along the radial direction). This is mainly motivated by understanding the particle dynamics in experiments carried out in spiral microfluidic channels, which reveal this channel to be very efficient for focusing/separating particles (inert or biological particles like algae or pathogens) when the inertia is finite at the particle scale (finite particle Reynolds number) [3, 4]. For fully understanding the particle dynamics, it is necessary to carefully investigate the single phase flow in this geometry, as this has been only partially addressed in the literature.

The flow in curved geometries exhibits recirculation in the cross-section, even in the

laminar regime. The first thoughts on this problem date back to Thompson in the 19th century [5]. Dean (1928)[6] established the first theoretical framework for fully developed pressure-driven flow in curved channels, by solving the Navier-Stokes equations based on a perturbation method. He demonstrated that secondary flows develop in the cross-section of a curved channel or pipe flow (rectangular or circular cross-section, respectively) in the form of two contra-rotating vortices. The flow solution, in the main and transverse directions, depends on a dimensionless parameter, which will be later called the Dean number, the product of the Reynolds number and the curvature ratio (the ratio between the characteristic size of the channel cross-section and the radius of curvature). In addition, the fluid dynamics in the laminar regime depends on the shape of the cross-section [7], as well as on rheological aspects for non-Newtonian fluids [8]. Subsequent numerical studies by Joseph *et al.* (1975) [9], Cheng *et al.* (1976) [10], Austin & Seader (1973) [11], to name a few, have focused on the developed laminar flows in rectangular curved channels. Other authors, such as Goldstein & Kreid (1967) [12], Ghia & Sokhey (1977) [13], Humphrey (1977) [14] and Hille & Schulz-Dubois (1985) studied flow development in curved square ducts combining both experimental and computational approaches for various Dean numbers. Afterwards, Berger *et al.* (1983) [15] provided an exhaustive and thorough review of theoretical and experimental studies on laminar incompressible flow in curved pipes.

In a curved rectangular channel, beyond a critical Dean number  $De_c$ , a second pair of vortices take place in the cross-section, due to an imbalance between pressure gradient and centrifugal forces near the outer curved wall [10]. This transition of secondary vortices from two-cells to four-cells has been studied in literature by Winters (1987) [16] who carried out the most complete bifurcation study in a curved channel of square cross-section. This work was followed later by Daskopoulos & Lenhoff (1989) [17], Kao (1992) [18], Bara *et al.* (1992) and Mees *et al.* (1996) [19] whose analysis covered different cross-sections and a large range of Dean numbers (up to  $De \approx 600$ ), reporting even the existence of transient six-cell flow state at very high Dean numbers. This rich literature reveals that the critical Dean number  $De_c$ , above which there is a transition from two- to four- or even six-cells, depends on the aspect ratio of the channel, see Fig. 10 in Fellouah *et al.* (2006) [20], and Kim & Borhan (2023) [21] .

In this work, we examine the fluid dynamics in a curved channel at low aspect ratio  $\lambda$ , setting it to 0.17 as explained earlier in the introduction. The aim of this work is to carefully examine the flow features in this case, from low to moderate Dean numbers, covering both fundamental fluid mechanics and engineering aspects. This investigation will be carried out with the aid of numerical simulations. We consider a curved channel with constant radius of curvature, so that numerical simulations can be carried out in small domains using periodic boundary conditions in the streamwise direction. In terms of geometry, the curved channel is similar to the annular plane Couette device [22], with the flow driven by a pressure gradient instead of a moving wall. In pressure-driven flow, the curved channel configuration is representative of bends in loops for fluid transport. As for spirals of Archimedean type used for instance in recent experiments [3, 4], the radius of curvature evolves continuously between the channel inlet and outlet. Except near the inlet, the curvature varies slowly along the azimuthal direction in those spiral devices, and therefore the change of curvature has a negligible influence on the flow features, as demonstrated by the theoretical work of Harding & Stokes (2018) [23]. In their work, the authors have derived solutions for pressure-driven fluid flow in planar spiral ducts with small aspect ratio ( $\lambda = 0.12 - 0.35$ ) and slowly varying curvature ratio. The authors found that the solution at leading order in  $\lambda$  and  $\delta$  depends only on the local curvature and not on its rate of change, as long as the Reynolds number remains moderate.

The paper is organized as follows. The flow equations are written in dimensionless form in Section II, allowing to discuss the contribution of inertial, centrifugal and viscous terms to the main and secondary flows as a function of the Reynolds number and the channel curvature. The numerical method is then succinctly presented in Section III. The primary and secondary flow are then characterized in Section IV and V. Then, Sections VII and VIII discuss the dimensionless friction factor and the entry length necessary for flow development, respectively, showing useful scaling laws for practical purposes. The paper ends with concluding remarks.

## II. DIMENSIONAL ANALYSIS

The fluid equations of motion satisfy the mass and momentum conservation, assuming the fluid flow is incompressible :

$$\nabla \cdot \mathbf{u} = 0, \quad (1a)$$

$$\frac{\partial \mathbf{u}}{\partial t} + (\mathbf{u} \cdot \nabla) \mathbf{u} = -\frac{1}{\rho} \nabla p + \nu \nabla \cdot (\nabla \mathbf{u} + \nabla \mathbf{u}^T) \quad (1b)$$

where  $\rho$  and  $\nu$  denote the fluid density and dynamic viscosity, while  $\mathbf{u}$  and  $p$  refer to the velocity and pressure fields, respectively. The body force associated with the fluid weight in the gravitational field is omitted here, as it has negligible contribution, especially when the dimensions of the channel are small. Otherwise, this force can be lumped into the vertical pressure gradient term, with no loss of generality.

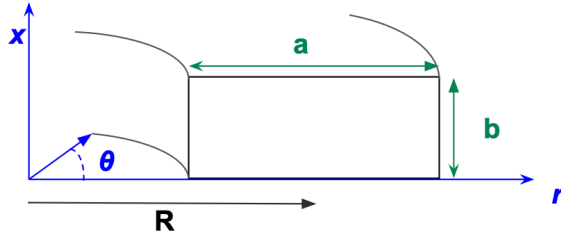


FIG. 1: Schematic representation of the flow geometry and the coordinate system.

To continue further, the equations are written in the Galilean frame of reference, using the cylindrical coordinates, shown in Figure 1.  $x$ ,  $r$  and  $\theta$  denote the axial, radial and tangential coordinates, respectively. The study is focused on channels with a rectangular cross-section of low aspect ratio,  $\lambda = \frac{b}{a} < 1$ , where  $b$  and  $a$  refer to the channel height and width in the axial and radial directions, respectively. The radius of curvature  $R$  denotes the distance between the axis and the centerline of the channel, and it is assumed constant in this work. To characterize the curvature, we use the curvature ratio  $\delta$  :

$$\delta = \frac{d_h}{2R};$$

with  $d_h = \frac{2ab}{a+b}$  being the hydraulic diameter. In addition, we introduce the ratio  $D = \frac{d_h}{a}$ , in which the hydraulic diameter is scaled by the channel width. In the limit  $\lambda \rightarrow 0$ , the hydraulic diameter approaches  $2b$  and therefore  $D \rightarrow 2\lambda$ . In order to write the flow equations of motion in a dimensionless way, the spatial coordinates, the velocity components  $v_r$ ,  $v_\theta$  and  $v_x$ , as well as the pressure field  $p$  are scaled as following:

$$\bar{r} = \frac{r-R}{a}; \quad \bar{x} = \frac{x}{b};$$

$$\bar{v}_r = \frac{v_r}{U_0}; \quad \bar{v}_\theta = \frac{v_\theta}{U_0}; \quad \bar{v}_x = \frac{v_x}{U_0}; \quad \bar{p} = \frac{p}{\rho U_0^2}$$

where  $U_0$  denotes the average velocity.

The flow will be fully characterized using the Reynolds number  $Re$  as usual in pipe flows, and the Dean number  $De$  to account for curvature. The Dean number is interpreted as the ratio between the square root of the inertial and centrifugal forces over the viscous force. Various definitions of the Dean number can be found in the literature, most of them being compiled by Berger *et al.* [15] and more recently by Saffar *et al.* [24] in the frame of microfluidic applications. In the present study, the following definition is used:

$$Re = \frac{\rho U_0 d_h}{\mu}; \quad De = Re \sqrt{\delta};$$

The dimensionless mass and momentum conservation equations become:

$$\frac{\lambda}{r^*} \frac{\partial}{\partial \bar{r}} (r^* \bar{v}_r) + \frac{\partial \bar{v}_x}{\partial \bar{x}} = 0 \tag{2a}$$

$$\bar{v}_r \frac{\partial \bar{v}_r}{\partial \bar{r}} - \frac{2}{D} \frac{\delta}{r^*} \bar{v}_\theta^2 + \frac{\bar{v}_x}{\lambda} \frac{\partial \bar{v}_r}{\partial \bar{x}} = -\frac{\partial \bar{p}}{\partial \bar{r}} + \frac{1}{Re} \left[ 2\delta \frac{\partial}{\partial \bar{r}} \left( \frac{\bar{v}_r}{r^*} \right) + D \frac{\partial^2 \bar{v}_r}{\partial \bar{r}^2} + \frac{D}{\lambda^2} \frac{\partial^2 \bar{v}_r}{\partial \bar{x}^2} \right] \tag{2b}$$

$$\bar{v}_r \frac{\partial \bar{v}_\theta}{\partial \bar{r}} + \frac{2}{D} \frac{\delta}{r^*} \bar{v}_r \bar{v}_\theta + \frac{\bar{v}_x}{\lambda} \frac{\partial \bar{v}_\theta}{\partial \bar{x}} = -\frac{1}{r^*} \frac{\partial \bar{p}}{\partial \theta} + \frac{1}{Re} \left[ 2\delta \frac{\partial}{\partial \bar{r}} \left( \frac{\bar{v}_\theta}{r^*} \right) + D \frac{\partial^2 \bar{v}_\theta}{\partial \bar{r}^2} + \frac{D}{\lambda^2} \frac{\partial^2 \bar{v}_\theta}{\partial \bar{x}^2} \right] \tag{2c}$$

$$\bar{v}_r \frac{\partial \bar{v}_x}{\partial \bar{r}} + \frac{\bar{v}_x}{\lambda} \frac{\partial \bar{v}_x}{\partial \bar{x}} = -\frac{1}{\lambda} \frac{\partial \bar{p}}{\partial \bar{x}} + \frac{1}{Re} \left[ D \frac{\partial^2 \bar{v}_x}{\partial \bar{r}^2} + \frac{2\delta}{r^*} \frac{\partial \bar{v}_x}{\partial \bar{r}} + \frac{D}{\lambda^2} \frac{\partial^2 \bar{v}_x}{\partial \bar{x}^2} \right] \tag{2d}$$

where  $r^* = (1 + 2\frac{\delta}{D}\bar{r}) \simeq 1$  when the ratio  $\frac{\delta}{D}$  is small (for large radius of curvature).

From eqs. 2, it can be already noted that at low Dean number, the viscous and centrifugal terms are of the same order of magnitude while the inertial terms are small, and the radial

dimensionless velocity  $\bar{v}_r$  is of  $O\left(\frac{\lambda^2}{D^2} Re\delta\right)$ . At moderate Dean numbers, the inertial and centrifugal terms are of the same order of magnitude and  $\bar{v}_r = O\left(\sqrt{\frac{\delta}{D}}\right)$ , while the viscous terms have negligible contribution outside the boundary layer near the walls.

### III. NUMERICAL METHOD

The numerical simulations of single-phase flow in a curved channel were carried out with the in-house JADIM code [25][26], designed to solve the three dimensional unsteady Navier-Stokes equations on curvilinear orthogonal grid. The flow equations of motion are spatially discretized over a staggered grid and integrated using a finite-volume method, and advanced in time via three-step Runge-Kutta procedure where nonlinear terms are explicitly computed and the linear diffusive terms are handled semi-implicitly by a Crank-Nicolson scheme. Incompressibility is enforced at the end of the complete time step through a projection technique. Centered schemes are used to evaluate the spatial derivatives. The corresponding solution of the Navier-Stokes equations is second-order accurate in space and time on a uniform grid.

No-slip boundary condition is imposed at the channel walls, and periodic boundary conditions are applied for the velocity and perturbed pressure along the azimuthal (streamwise) direction. At the start of a simulation, the fluid is at rest. A pressure gradient is then imposed in the streamwise direction to induce the flow. The convergence to a fully steady and developed flow is obtained once the residuals of the velocity components tend towards small relative values (of the same order or less than  $10^{-5}$ ). The evolution of the average flow velocity is recorded in time. The steady streamwise velocity, and subsequently the Reynolds numbers are determined *a posteriori*, once the simulation reaches the steady state.

A uniform grid is used for the simulations. The independence of the results on the mesh was ensured by testing four different grids described in table III included in the appendix XIA, with  $N_x$ ,  $N_r$  and  $N_\theta$  denoting the number of grid points along the channel height, width and length, respectively. It should be noted that only a small section of the curved channel is considered in the numerical simulations, i.e., the total angle of the simulated do-

main is specified ( $\Delta\theta = 5^\circ$ ), taking advantage of the periodicity in the azimuthal direction. Therefore, the mesh used in this work is significantly finer than in previous studies (for instance [20][27]).

Numerical simulations were carried out with a mesh resolution of  $(N_r, N_\theta, N_x) = (240, 16, 40)$ , for five curvature ratios summarized in table I. The smallest curvature ratios  $\delta_4$  and  $\delta_5$  correspond to the curvature ratio  $\delta$  of the smallest and largest loop of the microfluidic chips (Epigem) used for inertial focusing in [3, 4], which consists of a 6-turn Archimedean spiral. Larger curvature ratios are interesting for experimental setups at larger scales [20][14][28]. For each curvature ratio, simulations are carried out with different Reynolds numbers, in a way to cover Dean numbers between 1 and 200 approximately.

TABLE I: The five curvature ratios considered in the simulations of the present work.

$\delta_1$	0.14
$\delta_2$	0.089
$\delta_3$	0.053
$\delta_4$	0.039
$\delta_5$	0.006

In the following sections, we present the effect of inertia and curvature on the primary and secondary flows, while varying the Dean number from small to moderate values. Directly related to the flow velocity is the friction factor which is also calculated.

#### IV. GENERAL FLOW FEATURES

Figure 2 displays the contours of the dimensionless azimuthal velocity  $\bar{v}_\theta$  in the channel cross section, as well as the streamlines of the transverse velocities, once the steady state is reached. The rows of this figure correspond to curvature ratios  $\delta_1, \delta_4$  and  $\delta_5$ , respectively, and the columns correspond to  $De \sim 1, \sim 100$  and  $\sim 200$ , respectively.

First let's examine the results at low Dean number. At high curvature (Fig.2a), the maximum azimuthal velocity  $\bar{v}_\theta$  as well as the centers of the secondary vortices are located near the inner wall. At smaller curvature however, this maximum shifts to the middle of the

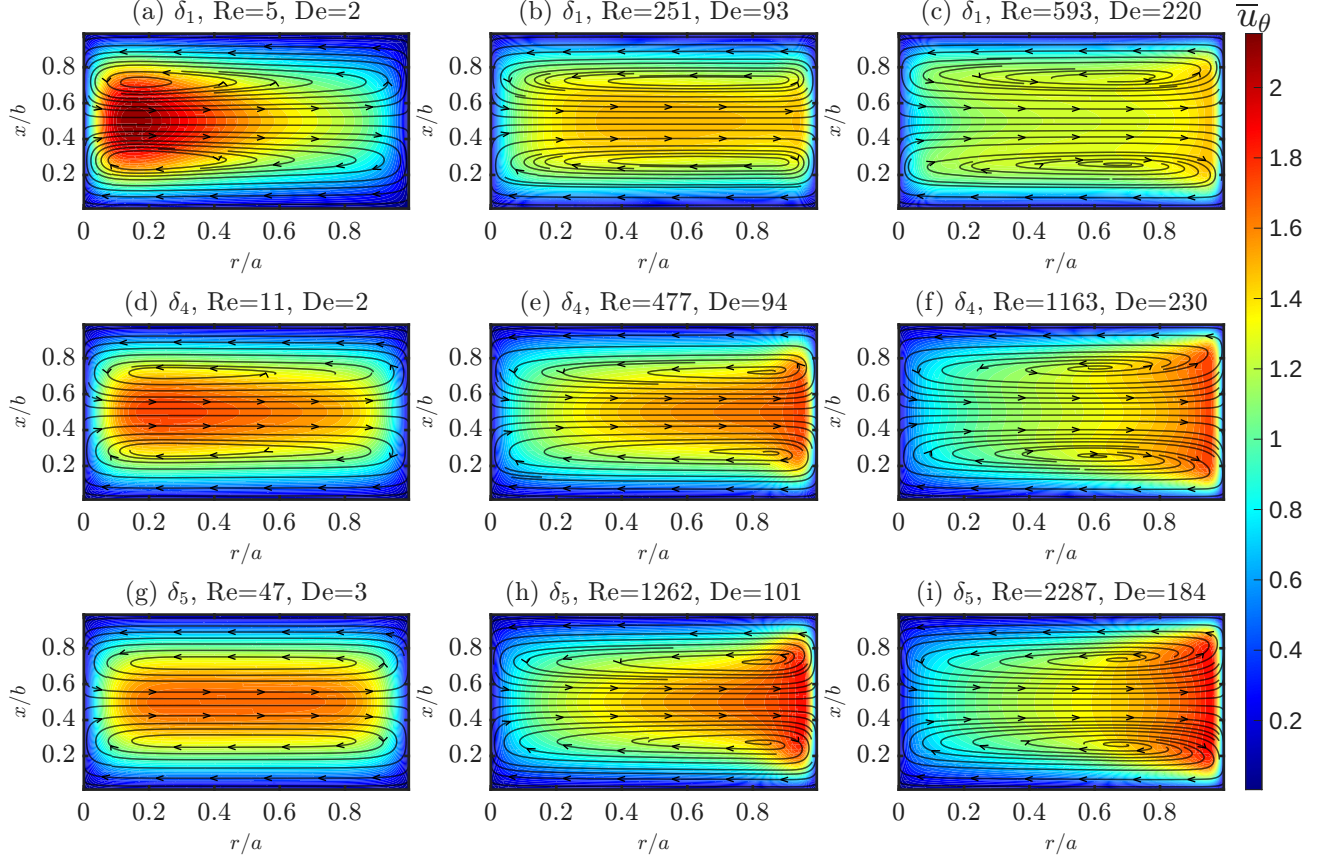


FIG. 2: Contours of the azimuthal velocity  $\bar{u}_\theta$  for various Dean numbers and curvature ratios. The streamlines indicate secondary vortices in the cross-section. Note that the aspect ratio of the channel cross-section is  $\lambda = 0.17$ .

channel (Fig.2g), similarly to the flow in a straight rectangular channel. As the Dean number increases, the secondary flow becomes stronger and both the peak of the streamwise velocity as well as the center of the secondary vortices shift towards the outer wall (Fig.2 (c,f,i)).

Already at this stage of observation, our results confirm, what is known in curved channel or pipe flows [15], that the secondary flows are not fully characterized by the Dean number and that other parameters such as the curvature ratio and the aspect ratio are key parameters to fully characterize the flow structure. In the following, we will add few comments on the main and secondary flow features.

It is not common to find the peak of the streamwise velocity closer to the inner wall of a curved pipe or channel flow, since this occurs only at weak inertia. In the case where  $\lambda \rightarrow \infty$ , the parallel flow solution (with no secondary flow) is a shifted parabola toward the

inner wall, sometimes referred to as CCPF (curved channel Poiseuille flow) [29], as long as inertial effects are weak. While the velocity peak shifts from the inner wall to the outer wall as the Dean number is increased at large curvature, the pressure gradient in the radial direction remains positive for all curvature ratios and Dean numbers. The pressure peak falls at the outer wall independent of the operating conditions (see Appendix XI B).

At the highest Dean numbers,  $De \sim 200$ , we do not observe additional pair of secondary vortices. The experiments of Sugiyama *et al.* [30] suggested that the critical Dean number, above which two pairs of secondary vortices occur instead of one pair, is  $De_c \sim 100$  for  $\lambda = 0.5$ . They also suggested that  $De_c$  increases when the channel aspect ratio decreases. Extrapolating their results to lower aspect ratio, this is consistent with our results. Recently, the work of Kim *et al.* [21] based on numerical simulations showed that the critical Dean number, above which two pairs of secondary vortices are observed, obeys the following empirical law:  $\lambda^{1/2}De_c \sim 110$ . Our simulations agree with their finding, as the product  $\lambda^{1/2}De$  is smaller than 110, at the largest Dean numbers considered. This finding contradicts with the work of Nivedita *et al.* [31], who observed based on fluorescence (with relatively low resolution) that two pairs of secondary vortices occur at lower Dean numbers  $De_c \sim 40$ . It is not possible to comment further on this disagreement, as to the authors' knowledge, there is no other work that show such transition at relatively low Dean number.

At large curvature ratio and for sufficiently large Dean numbers, transient structures take place in the flow (see Appendix XI C for  $\delta_1$  and  $De \sim 230$ ) once the flow has traveled a long distance, i.e. travel angle larger than  $\approx 10\pi$  which corresponds to several turns if the channel was infinitely long with a small variation of the radius of curvature. One example of the flow structure is further discussed in appendix XI C. We did not investigate thoroughly the flow transition, as it is out of the scope of the present work, but we expect that the transition angle  $\theta_t$ , when transition occurs, should depend on both the curvature ratio and the Reynolds (or Dean) number. For instance for  $\delta_1$ , these structures have appeared at shorter time in comparison with smaller  $\delta$ .

Next, we show quantitative features of the primary and secondary flow, based on velocity profiles. Furthermore, some velocity gradient profiles are also included in section XI A, in the frame of the numerical tool validation.

## V. VELOCITY PROFILES

Figure 3 displays the radial profile of the dimensionless azimuthal velocity along the mid-plane  $\bar{x} = 0.5$  in the channels of curvature ratio  $\delta_4$  and  $\delta_5$  for various Reynolds numbers. Those profiles evidence the existence of a local velocity maximum near the inner wall of the channel of curvature ratio  $\delta_4$  and the shift of the velocity maximum toward to the outer wall when the Reynolds number increases. In addition, we note that at high Reynolds (or Dean) numbers, the maximum is located at a distance  $\approx b/4$  from the outer wall. The same conclusions can be drawn for  $\delta_5$ , although the velocity profiles at low De are flatter than those reported for  $\delta_4$ .

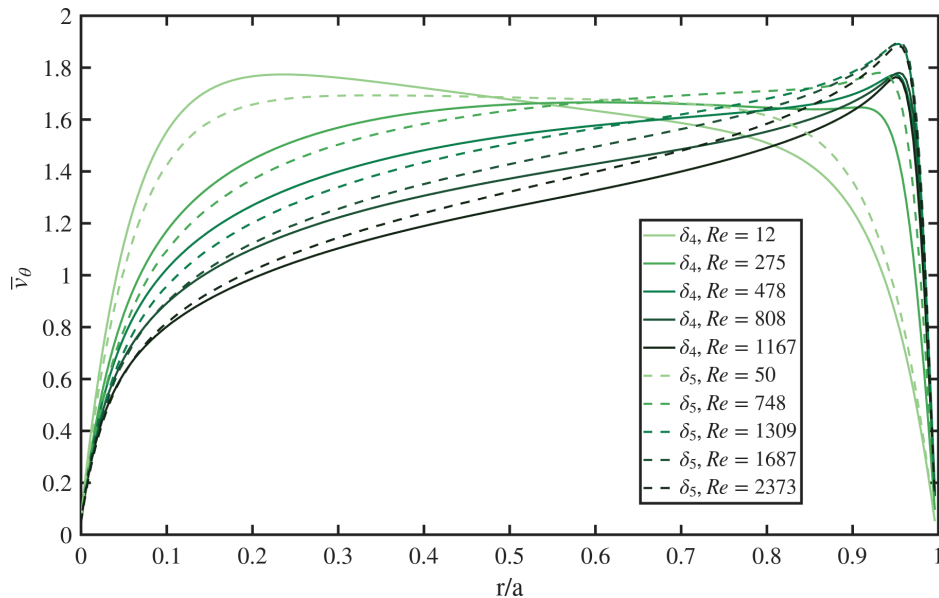


FIG. 3: Profiles of the dimensionless tangential velocity  $\bar{v}_\theta$  along the mid-plane  $\bar{x} = 0.5$  for various Re and curvature ratios. Solid and dashed lines correspond to  $\delta_4$  and  $\delta_5$ , respectively.

Next, to better characterize the secondary flow, we consider the profile of the radial velocity  $\bar{v}_r$ , for instance along the axial direction, as displayed in Fig. 4a at the medium plane  $\bar{r} = 0$ . As expected from the shape of secondary vortices, the radial velocity is positive near the midplane ( $\bar{x} = 0$ ), as it is oriented from the inner to the outer wall, and it is negative near the top and bottom walls. This figure shows also that scaling the radial velocity with  $\delta Re \lambda^2$  at small Dean number ( $De \leq 50$ ), allows not only to collapse all the profiles, but the amplitude of radial velocity approaches  $O(1)$ . Moreover, at moderate Dean numbers ( $50 \leq De \leq 250$ ),

Fig. 4b shows that the radial velocity scales reasonably well like  $\sqrt{\delta}$  which also aligns with the dimensional analysis presented in section II. The fact that the curves do not collapse on a single master trend suggests that  $\bar{v}_r$  should also depend on the Reynolds number in addition to  $\delta$ . This will be discussed in the next section, considering the average amplitude of the secondary flow intensity.

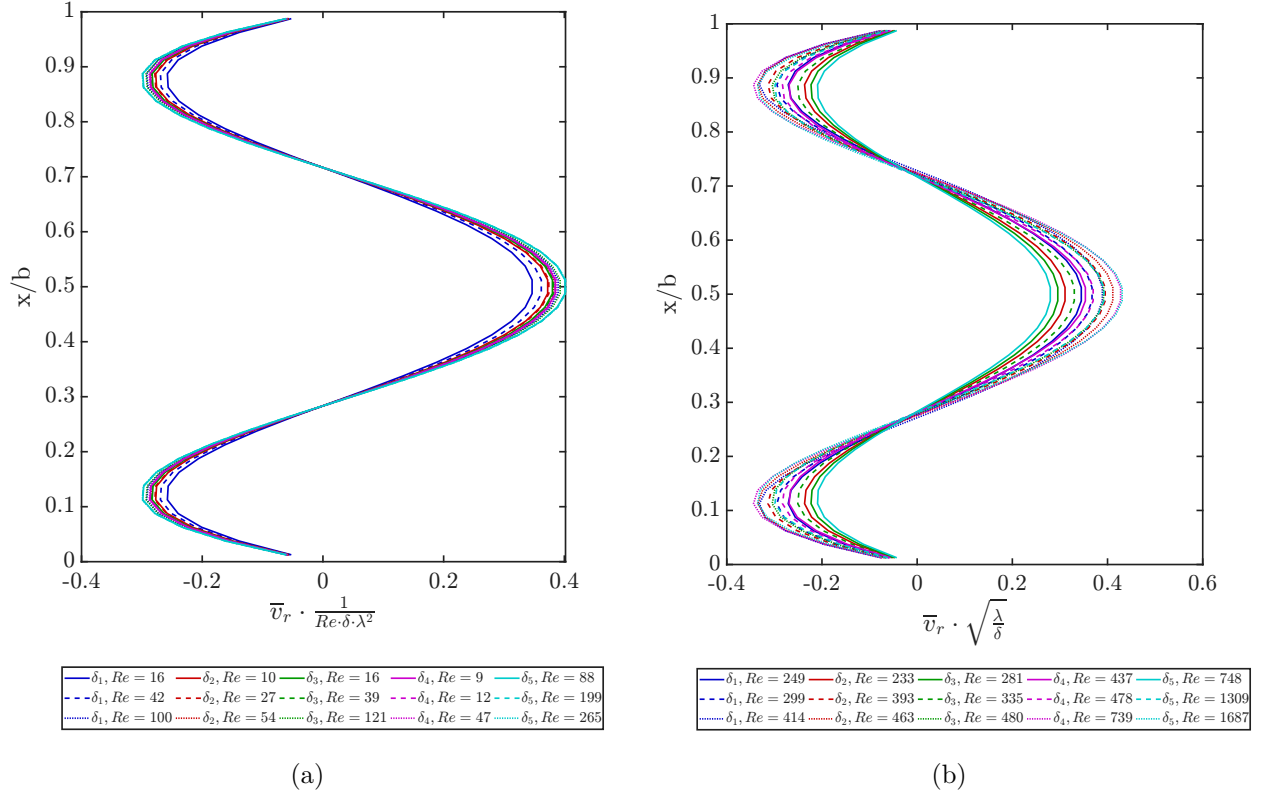


FIG. 4: Axial profiles of the radial velocity  $\bar{v}_r$ , along the mid-plane  $\bar{r} = 0$  for various curvature ratios at (a) low De and (b) moderate De.

## VI. INTENSITY OF SECONDARY FLOWS

In the cross-section of a curved channel flow, the velocity field takes the form of secondary vortices which intensity increases with the flow inertia. It is important to understand how secondary flows scale with the dimensionless parameters, as they ensure mixing in the cross-section. At low Dean numbers, scaling in the form of power law have been suggested in the literature [32]. At higher Dean numbers (up to 100), and using exact mathematical solution of the Navier-Stokes equations, Harding [33] has shown that a simple power law scaling does

not hold in the entire range of Dean numbers, suggesting another scaling, in the form of the inverse of a polynomial function. Using numerical simulations, we will show that, following the dimensional analysis, one can find the correct scaling of the secondary flow in different regimes, dominated by either viscous or inertial effects.

The intensity of the secondary flow is defined from the root mean square of the radial and axial velocities:

$$I = \frac{\left\langle \sqrt{v_r^2 + v_x^2} \right\rangle}{U_0} \equiv \left\langle \sqrt{\bar{v}_r^2 + \bar{v}_x^2} \right\rangle,$$

where the brackets denote the average over the cross-section. Fig. 5a shows the secondary flow intensity  $I$  as a function of the Dean number for different curvature ratios. At low to moderate Dean numbers, the intensity of secondary flows increases with the Dean number. As  $I$  increases progressively starting from zero, this suggests the absence of bifurcation at low Dean numbers. The curves tend to level off starting from  $De \sim 100$ . The plateau depends on the channel curvature: the stronger the curvature, the higher is the asymptotic value of the intensity  $I$ . When  $\delta$  increases from 0.006 to 0.14, the intensity of secondary flows increases from 4 to 18% of the average flow velocity.

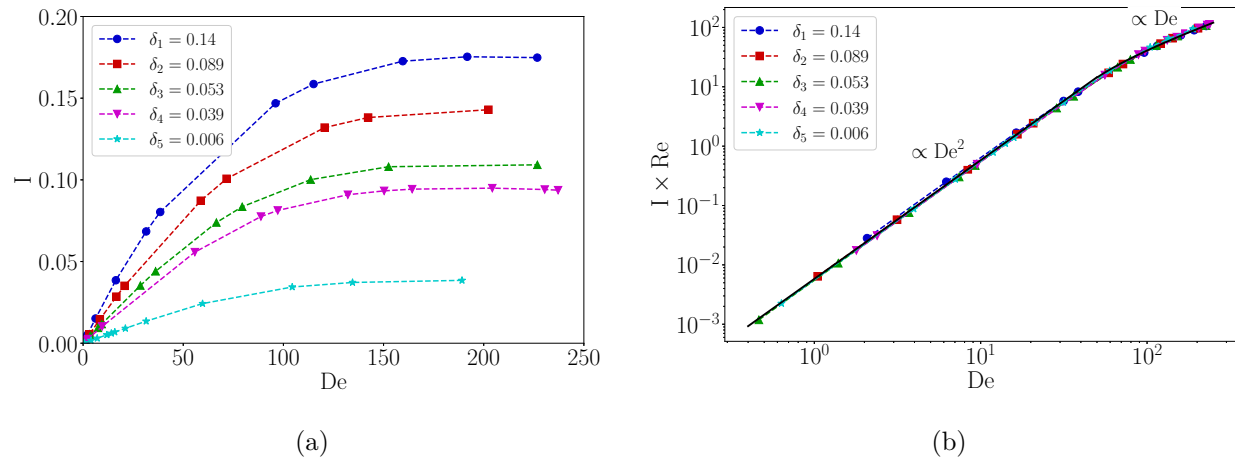


FIG. 5: Secondary flow intensity as a function of the Dean number.

5b shows that, when plotting  $I \times Re$  as a function of the Dean number  $De$ , the curves corresponding to different curvatures collapse onto a master curve. This figure shows that there are clearly two trends when the Dean number is increased. At low Dean numbers,  $I \times Re$  scales like  $De^2$  or equivalently  $I \propto \delta Re$ , whereas at moderate Dean numbers,  $I \times Re$

scales rather like  $De$  or in an equivalent way  $I \propto \sqrt{\delta}$ . Two scaling laws are suggested in eq. 3, and are added to Fig.5b within the corresponding range.

$$I = \frac{1}{Re} (6 \times 10^{-3} De^2) \text{ for } De < 50, \quad (3a)$$

$$I = \frac{1}{Re} (0.53 De - 10.6) \text{ for } 50 < De < 250 \quad (3b)$$

The trends identified here are in agreement with the scaling analysis discussed in section II. While the contribution of the inertial terms to the momentum balance along the radial and axial directions (eqs. 2) is weak at low Dean numbers, the viscous and curvature terms balance each other, leading the dimensionless secondary velocity (components  $\bar{v}_r$  and  $\bar{v}_x$ ) to scale like  $\delta Re$ . However, at moderate Dean numbers, the viscous terms have negligible contributions to the momentum balance, and thus the dimensionless secondary velocity is expected to scale like  $\sqrt{\delta}$ . It might seem surprising that the viscous scaling applies up to  $De \sim 50$ . We expect that this limit, as well as the constant appearing in the linear-like trend are dependent on the shape and dimension of the cross-section.

## VII. FRICTION FACTOR

Although interesting from practical point of view (for dimensioning purposes), recent investigations on the fluid flow in curved channels do not systemically report the pressure drop. This section aims thus to find a relationship between the pressure drop  $\Delta P/L$  in its dimensionless form via the friction factor  $f$ , the Dean number and the curvature. The friction factor  $f$  is defined as the ratio between the wall shear stress  $\tau_w = \frac{\Delta P}{L} \cdot \frac{d_h}{4}$  (this relation resulting from the macroscopic momentum balance), and the dynamic pressure, leading to  $f = \frac{\tau_w}{\frac{1}{2} \rho U_0^2}$ . Replacing the wall shear stress by the pressure drop, the friction factor can be written :

$$f_c = \frac{1}{2R} \frac{\Delta P}{\Delta \theta} \cdot \frac{\rho d_h^3}{Re^2 \mu^2} \quad (4)$$

where the index  $c$  refers explicitly to curved channels or pipes. The pressure drop in that case corresponds to  $\frac{\Delta P}{L} = \frac{\Delta P}{R\Delta\theta}$ , with  $\Delta\theta$  being the angle in radian across which the pressure drop is measured or imposed. Thus, for an imposed pressure drop  $\frac{\Delta P}{\Delta\theta}$  in the simulations, the average streamwise velocity (or equivalently Reynolds number) is calculated once the steady state is reached, and subsequently, the friction factor  $f_c$  is calculated following eq. 4. Then, the friction factor is scaled by the friction factor  $f_s$  in a straight channel of similar cross section. The latter is calculated from numerical simulations carried out in a straight channel (with  $\lambda = 0.17$ ) and compared with the Darcy Weisbach relation valid for laminar flow [34]:

$$f_s = \frac{k}{Re}$$

where  $k$  is a constant that depends on the shape and the aspect ratio of the channel cross-section ([34], p.387). For  $\lambda = 0.17$ , the friction factor in the straight channel is  $f_s = 19/Re$ .

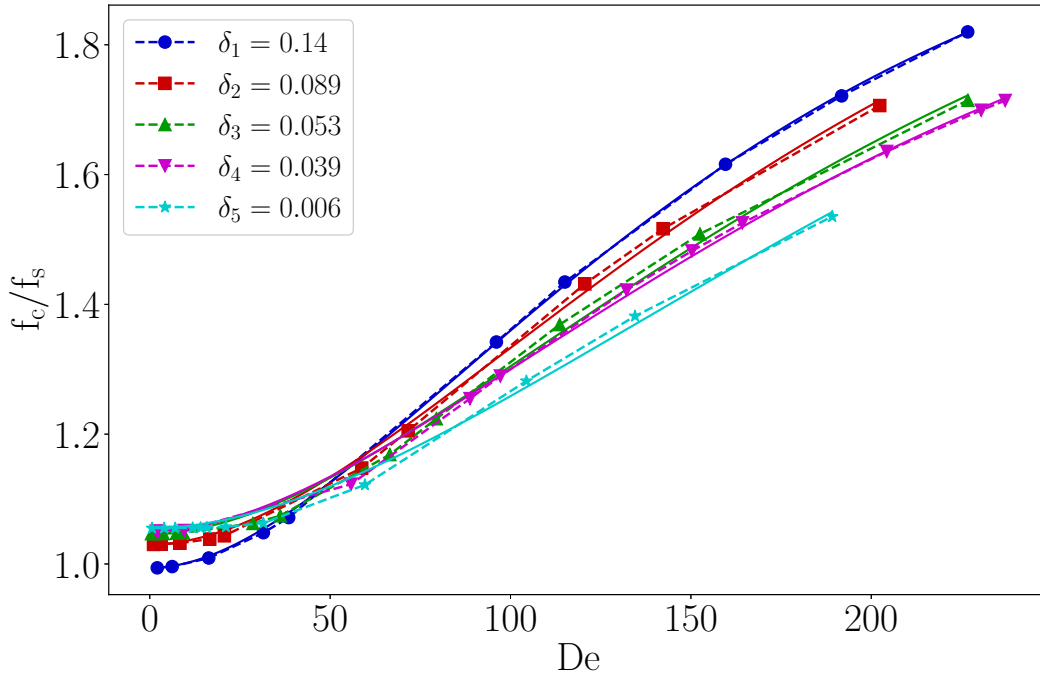


FIG. 6: Friction factor of the curved channel flow, rescaled by the friction factor of a flow in a straight channel of similar cross-section, as a function of Dean number for different channel curvatures (indicated by symbols). Solid lines are from eq. 5 and each color corresponds to one curvature ratio.

The rescaled friction factor  $f_c/f_s$  is displayed in Fig. 6 as a function of the Dean number, for different curvature ratio. This figure shows that the rescaled friction factor increases with the Dean number. Our simulations suggest that the additional dependence of flow resistance on the curvature ratio  $\delta$  is small beyond its dependence on the Dean number (which already includes the effect of curvature), in agreement with past studies in coiled pipes [11, 35]. The plots at different  $\delta$  follow the scaling law :

$$\frac{f_c}{f_s} = C + A \left[ 1 - \left( 1 + \frac{De}{\alpha} \right) \cdot \exp \left( \frac{-De}{\alpha} \right) \right] \quad (5)$$

where the parameters  $C = \left. \frac{f_c}{f_s} \right|_{De \rightarrow 0}$ ,  $A$  and  $\alpha$  depend on the curvature ratio. They are reported in table II.

TABLE II: Parameters of the normalized friction factor, eq. 5, for different curvature ratios.

	$C$	$A$	$\alpha$
$\delta_1$	0.99	1.1	84.44
$\delta_2$	1.03	1.12	98.86
$\delta_3$	1.04	1.09	108.12
$\delta_4$	1.05	1.01	105.12
$\delta_5$	1.055	1.18	133.78

When  $De \rightarrow 0$ , the rescaled friction factor  $f_c/f_s \rightarrow C \approx 1$ , and its dependence on the curvature ratio deserves some comments.  $C$  is slightly smaller than 1, or equivalently the friction coefficient in the curved channel flow is slightly smaller than the friction factor in straight channel at the highest curvature,  $\delta_1$ . Similar observations were reported in the past, for instance in coiled pipes, where the flow resistance for a strongly curved pipe is less than that of a loosely coiled one [36]. This effect can be attributed to the skewed streamwise velocity near the inner wall at large  $\delta$  and small Dean number, as shown in the panel at the top left corner of Fig. 2. Knowing that the surface of the inner wall is smaller than the surface of the outer wall in curved channels, the increase of the shear stress at the inner wall (compared to that on the wall of the straight channel) is thus compensated by the decrease of the inner wall surface, leading to a slightly smaller friction factor. On the contrary,  $f_c/f_s$

tends to  $\approx 1.05$  instead of 1 when the curvature is small. Several verification tests confirmed that this plateau is independent of the grid resolution in the three directions. At small  $\delta$ , the streamwise velocity is less skewed toward the inner channel wall, and since the surface of the outer wall is larger than the inner one, it leads to the slight increase of the friction factor compared to the straight channel flow.

### VIII. ESTIMATED ENTRY LENGTH

Like the dimensionless pressure drop, the entry flow is of practical importance as it gives insights on the distance required for the flow to become fully developed. An interesting picture of the flow development has been summarized by Berger et al. [15]. When a fluid is pumped in a pipe, the central core near the entrance is not influenced by the walls, unlike a thin layer near the wall that experiences viscous effects. The boundary layer develops initially like that in a straight pipe. Immediately downstream the entrance, the flow (in the streamwise direction) consists of two regions: the central region mainly experiences the centrifugal force (due to curvature) balanced by a radial pressure gradient, and the thin boundary layer where inertial and viscous forces balance each others. The inward pressure gradient induces a transverse flow in the boundary layer, in general from the outer wall toward the inner wall. The displacement effect in the boundary layer accelerates the flow in the core, while the secondary currents induce a flow from the inner to the outer wall. Those sequences occur up to a distance  $R\theta_e = O(d_h)$  (or equivalently  $\theta_e = O(\delta)$ ) from the entry, for any Dean number. Beyond this distance, the flow depends on the Dean number. On the one hand, for small Dean number, the centrifugal force remains of second order (as in the first in the initial  $O(\delta)$  region). The boundary layer continues to grow downstream until it fills the cross-section and the flow is fully developed. This length scale is  $R\theta_e = O(d_h Re)$  like in a straight pipe, or equivalently  $\theta_e = O(\delta Re)$ . On the other hand, for large Dean numbers, centrifugal effects are as important as viscous and inertial effects, since the entrance. Much of the flow development occurs within a distance  $R\theta_e = O(R\sqrt{\delta}) \ll O(d_h Re)$ , leading very short entry length in this case, compared to entry length in straight pipe.

From the numerical simulations, the entry length is calculated as following. The pressure drop is applied on the fluid initially at rest. The fluid flow evolves progressively until

reaching the steady state. Note that this temporal approach mimics the flow development by relating the non-linear streamwise development of the motion to the temporal one. Thus, the distance traveled by the fluid during the transient stage is equivalent to the establishment length scale. To estimate this establishment length, we have calculated the instantaneous streamwise velocity averaged over the cross-section. The transient time scale  $T_L$  is estimated from the time needed for the average velocity to reach 95% of its steady state value. The establishment length is thus calculated using  $R\theta_e = \int_{T_L} \langle v \rangle dt$ , with  $\theta_e$  referring to the angle (in radian) traveled by the fluid, on average, before the fluid becomes fully developed. This angle, called entry angle in the following, is plotted as a function of De in Fig. 7a. It is clear that the entry angle increases with the Dean number, as well as the curvature ratio. When multiplying  $\theta_e$  by Re, the curves collapse on a single global trend as illustrated in Fig. 7b. At small Dean numbers ( $De \leq 50$ ),  $\theta_e Re$  scales like  $De^2$  and therefore the entry angle scales like  $\delta Re$ , similarly to the flow in a curved pipe. However, at moderate Dean numbers ( $50 \leq De \leq 250$ ), we find that  $\theta_e Re$  scales like  $De^{1.5}$ , which suggests that the entry angle of order  $\delta\sqrt{\delta Re}$  still depends although weakly on the Reynolds number, unlike the scaling expected at large Dean numbers, i.e.  $\theta_e = O(\sqrt{\delta})$  [15].

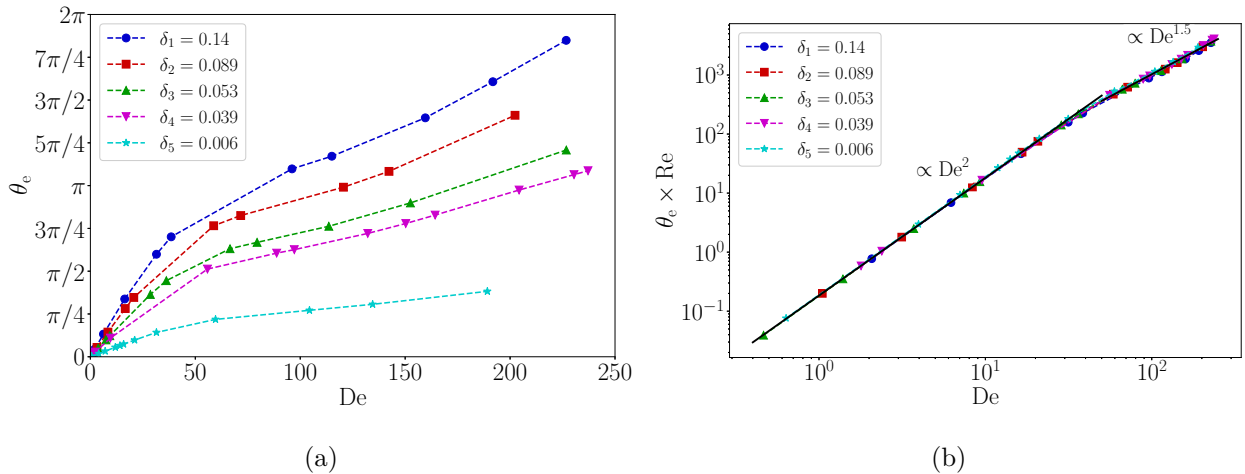


FIG. 7: a) The entry angle  $\theta_e$  as a function of the Dean number. In b) the entry angle is plotted in the form  $\theta_e Re$  on logarithmic scale. The  $De^2$  and  $De^{1.5}$  scaling at small and moderate Dean numbers, respectively, are added to this panel.

We would like to add two further comments on the entry length results. The flow in a curved pipe or channel at constant curvature is strictly valid for a total angle smaller than

$2\pi$ , which is the case of all the simulations realized for this work, according to Fig. 7a. Moreover, the entrance angle is smaller than  $\pi$  in most of the simulations, which would correspond to a  $180^\circ$  bend in a loop. The exact value of the entry angle depends on of the flow distribution at the entrance of the pipe, or on the flow state in the periodic simulations. In the present work, we calculated the distance traveled on average by the fluid starting from rest and converging in time to the stationary velocity. In a similar manner in experiments, the flow usually enters a pipe at a given flow rate, and the establishment length corresponds to the distance traveled by the fluid before converging toward the configuration associated with the pipe boundary conditions. In the case of a spiral channel where the curvature continuously increases along the flow direction, our results suggest that the flow adapts to the curvature change within small angles, in the range of curvature ratios and Dean numbers investigated in this work.

## IX. CONCLUDING REMARKS

This paper investigated the flow dynamics in curved channels with small aspect ratio,  $\lambda = 0.17$ , from low to moderate Dean numbers ( $De \lesssim 250$ ) and for a wide range of curvature ratios ( $0.005 \leq \delta \leq 0.15$ ). The numerical investigation was carried out in curved channels with periodic boundary conditions in the streamwise direction considering constant radius of curvature. The flow analysis was done at steady state, that takes place before the flow travels one complete turn, for all the curvature ratios and Dean numbers. At a given Dean number, the analysis evidenced that the primary flow and secondary vortices are highly dependent on the curvature ratio, confirming that the Dean number is not sufficient for fully characterizing the flow dynamics.

At low Dean number and high curvature ratio, the peak of the streamwise velocity is located near the inner wall. When the Dean number is increased and/or the curvature ratio is decreased, the velocity peak shifts progressively toward the outer wall. As a preamble to future works, we would like to stress that the alteration of the velocity peak along the radial direction (from near inner to near outer wall), can significantly impact hydrodynamic forces experienced by particles transported by the flow at low volume fractions.

As for the transverse velocities, we have only observed one pair of secondary vortices, as long as the flow remained stationary. The intensity of the secondary flows experienced two different scalings across the considered range of Dean numbers. At low Dean numbers ( $De \leq 50$ ),  $I \propto \delta Re$  as the viscous and centrifugal terms, are of the same order of magnitude, in the radial momentum conservation equation. However, at moderate Dean numbers ( $50 \leq De \leq 250$ ),  $I \propto \sqrt{\delta}$  as the inertial terms become dominant and of the same order of magnitude as the centrifugal term. The same scaling holds for radial velocity profiles when plotted along the axial direction. In transport applications, this scaling is useful to predict the drag and mixing time in the cross-section of curved channel flow.

The paper ends with scaling laws for the friction coefficient (dimensionless pressure-drop) and the entrance length or angle. The friction coefficient scaled by the friction coefficient of the flow in a straight duct of similar cross-section, exhibits two trends. At small Dean numbers, this ratio does not significantly depend on the Dean number, and it slightly decreases with  $\delta$ . At moderate Dean numbers, however, this ratio mainly increases with the Dean number and it slightly increases with  $\delta$ . The entrance length required for the flow to become established, starting from rest, is assessed by measuring the angle of development  $\theta_e$ . Two distinct regimes are observed: at low Dean numbers  $\theta_e \propto \delta Re$ , consistent with the entry angle in curved pipe flow, while at moderate Dean numbers we found that  $\theta_e \propto \delta \sqrt{\delta Re}$ .

While these results stem from simulations of a fluid flow induced by a pressure gradient, we expect that the conclusions also apply for flow in spiral channels with continuously increasing or decreasing radius of curvature, with small curvature variation along the flow direction, especially when the inertial effects are relatively weak, at low Dean numbers ( $De \leq 50$ ), in agreement with the mathematical analysis of [23]. At larger Dean numbers, the (in)dependence of the results on the curvature variation has yet to be discovered.

## X. ACKNOWLEDGMENT

This research was carried as part of the project Posseidon-TIRIS co-funded by ANR under France 2030 program (ANR-22-EXES-0015), the Occitanie Region and the European Regional Development Fund. Computational resources were provided by the meso-centre

## XI. APPENDIX

### A. Accuracy of numerical solution

We have carried out several tests in order to check the numerical accuracy of the code Jadim for solving curved channel flows. Table III summarizes the tests in the case of a curvature ratio  $\delta = 0.14$  and a rectangular cross-section with  $\lambda = 0.17$  and a total angle of  $5^\circ$  in the azimuthal direction. The Dean number is equal to 117 in that case.

TABLE III: Distribution of the mesh in different directions.

	$N_x$	$N_r$	$N_\theta$	Number of cells	$I$	$\frac{f_c}{f_s}$
mesh 1	40	240	16	153600	0.1629	1.476
mesh 2	40	360	16	460800	0.1629	1.476
mesh 3	50	400	16	320000	0.1628	1.458
mesh 4	50	480	16	768000	0.1628	1.458

Fig. 8 illustrates the profiles of the dimensionless streamwise velocity  $\bar{v}_\theta$  and its gradient along the radial and axial directions, as well as the radial velocity  $\bar{v}_r$ . Those profiles have been chosen since they involve the main quantities explored in this work, especially the velocity and friction factor. Those profiles are almost overlapping, which suggest that the smallest grid resolution is already sufficient for studying rigorously the flow in the geometry of interest.

Furthermore, the dependence of the results on the domain length was tested by changing the curvature angle of the channel as reported in table IV. For the same grid size, the simulation results are independent of the domain length, hence the choice of a small curvature angle of  $5^\circ$  for computational efficiency.

### B. Radial pressure gradient

Fig. 9 displays the radial pressure gradient along the radial direction. This figure confirms that the pressure gradient is positive for all curvature ratios and Dean numbers. Note that

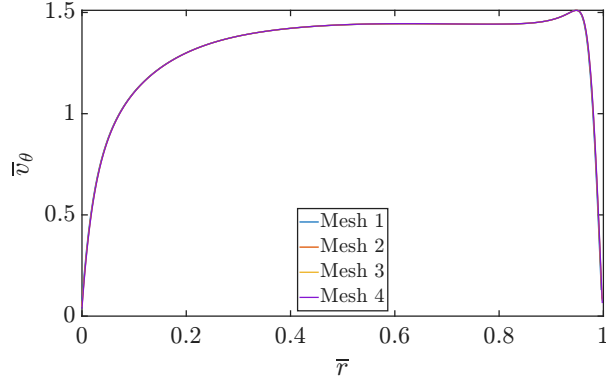
TABLE IV: Mesh grids for various domain angle

	$N_x$	$N_r$	$N_\theta$	$\theta$	$I$	$\frac{f_c}{f_s}$
mesh 1	40	240	16	5°	0.1629	1.4760
mesh 5	40	240	32	10°	0.1629	1.4760
mesh 6	50	400	64	20°	0.1629	1.4760

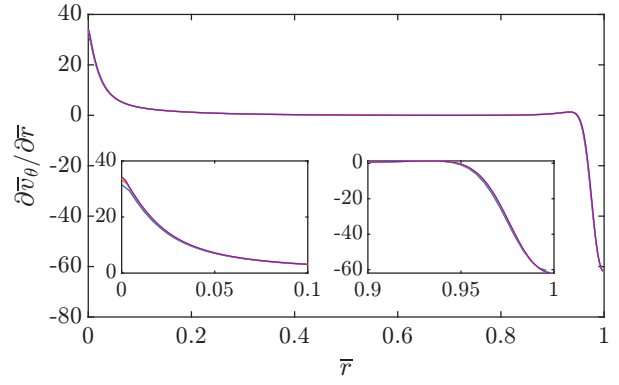
the pressure is scaled by the dynamic pressure, whereas the differential radius is scaled by the channel width. The dimensionless radial pressure gradient is then multiplied by  $1/\delta$  in order to compare profiles from different curvatures. At high curvature ratio and/or low Dean number, the radial pressure gradient, like the streamwise velocity profile (Figs. 2 and 3), exhibits an extremum near the inner wall. This is not surprising since the centrifugal force acts as a source term in the momentum conservation equation, and the pressure gradient and viscous (resp. inertial) terms follow similar evolution in the cross-section. As the curvature ratio decreases and the Dean number increases, the local extremum shifts toward the outer wall, which is very similar to the shift of the peak of the streamwise velocity.

### C. Instabilities at high Dean number

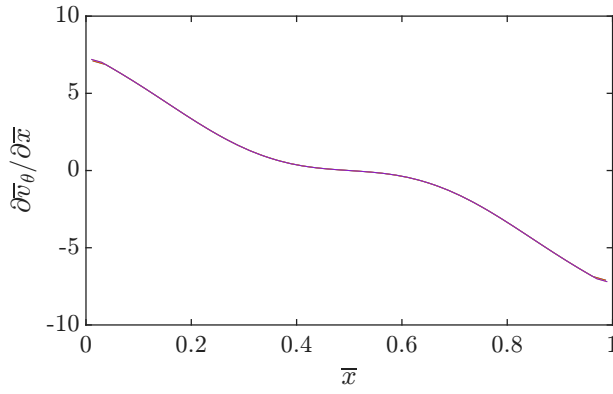
In all the results shown in this work, the flow remained steady while traveling for at least  $10\pi$ . At high Dean numbers and high curvature ratio, the flow is not unconditionally stable. Indeed, when flow inertia is relatively strong, perturbation of numerical nature grows in time without being dissipated by viscous effects. Fig.10 shows an example ( $De \gtrsim 200$  and  $\delta_1$ ) where the flow becomes unstable once it has traveled, on average, an angle of  $\theta \sim 20\pi$ . This instability takes the form of an elongated wave propagating in the cross-section similarly to what has been described by [37] in the case of rotating curved channel flow. In their case, the Coriolis force comes into play, in addition to the centrifugal force, and depending on the direction of the rotation of the flow, the instabilities due to Coriolis and centrifugal effects interact to either cancel or enhance each other [37]. It is interesting to observe similar motion of the transient structures even in the absence of Coriolis forces.



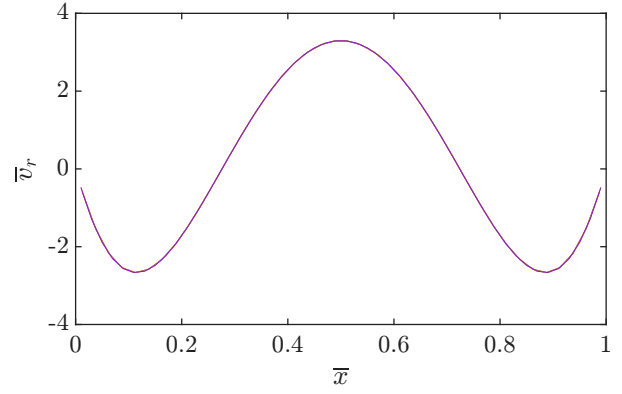
(a) Non-dimensional tangential velocity  $\bar{v}_\theta$  profile along the mid-plane  $\bar{x} = 0.5$



(b) Radial gradient of the tangential velocity  $\partial\bar{v}_\theta/\partial\bar{r}$  along the mid-plane  $\bar{x} = 0.5$



(c) Axial gradient of the tangential velocity  $\partial\bar{v}_\theta/\partial\bar{x}$  along the mid-plane  $\bar{r} = 0.5$



(d) Non-dimensional radial velocity  $\bar{v}_r$  profile near the inner wall  $\bar{r} = 0.9$

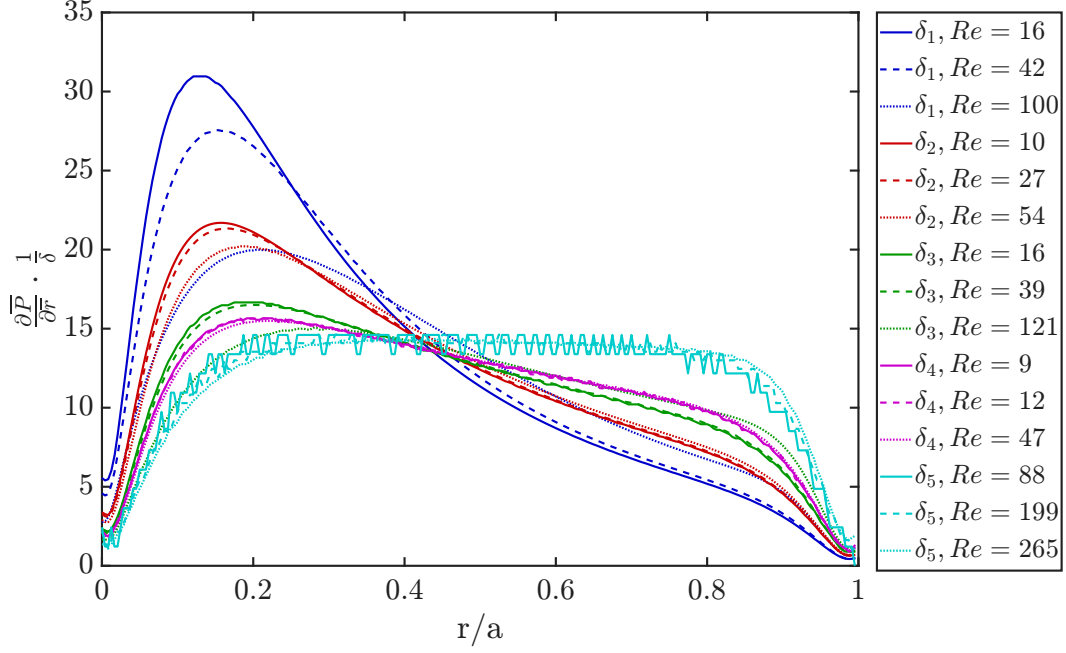
FIG. 8: Dependence on the grid resolution of the dimensionless profiles of the a) streamwise velocity, b) radial and c) axial gradient of the streamwise velocity, and d) radial velocity. The simulations were carried out in curved channel flow with  $\delta_1$  and  $De = 117$ . The mesh distribution is given in table III.

- 
- [1] J. Martel and M. Toner, Particle focusing in curved microfluidic channels, *Scientific Reports* **3**, 3340 (2013).
- [2] R. Valani, B. Harding, and Y. Stokes, Bifurcations in inertial focusing of a particle suspended in flow through curved rectangular ducts, in *Dynamical Systems Theory and Applications* (Springer, 2021) pp. 667–683.

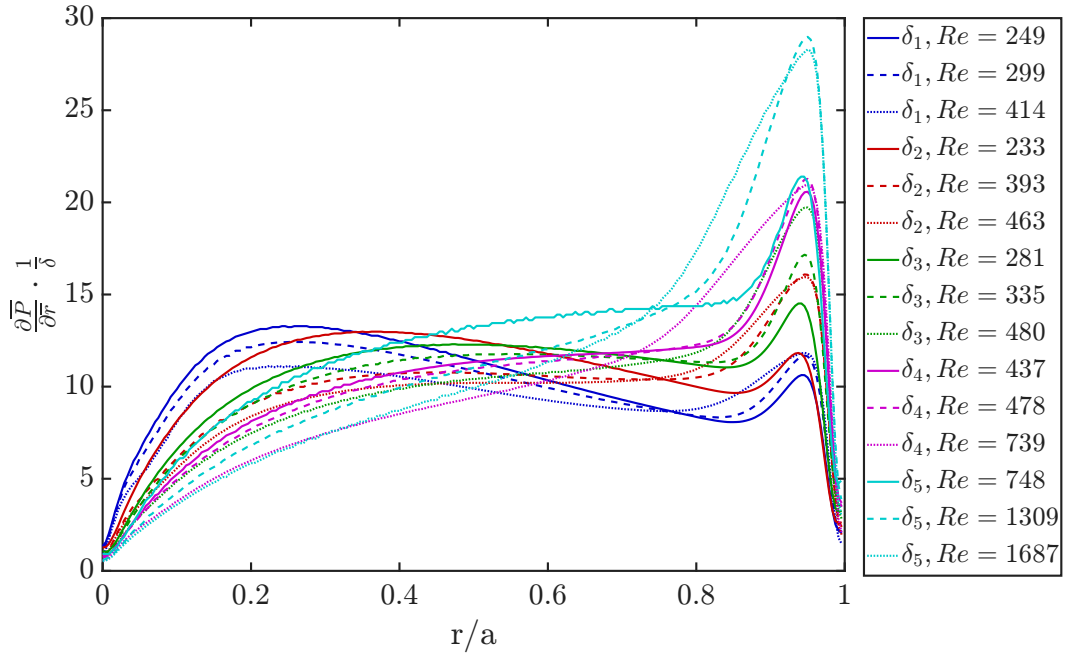
- [3] J. Howell, N. Hall, S. Omwenga, T. Hammarton, and M. Jimenez, An experimental investigation into the focusing behaviours of flagellated and elongated cells in inertial microfluidic devices, *Analyst* **150**, 3602 (2025).
- [4] C. Hill, N. Willoughby, and H. Bridle, Efficient high-concentration dewatering of chlorella vulgaris utilising spiral inertial microfluidics, *Bioresource Tech. Rep.* **18**, 101014 (2022).
- [5] J. Thomson, On the origin of windings of rivers in alluvial plains, with remarks on the flow of water round bends in pipes, *Proceedings of the Royal Society of London* **25**, 5 (1877).
- [6] W. R. Dean, Fluid motion in a curved channel, *Proceedings of the Royal Society of London. Series A, Containing Papers of a Mathematical and Physical Character* **121**, 402 (1928).
- [7] H. G. Cuming, *The Secondary Flow in Curved Pipes*, Reports and Memoranda 2880 (Aeronautical Research Council, 1952).
- [8] R. H. Thomas and K. Walters, On the flow of an elastico-viscous liquid in a curved pipe of elliptic cross-section under a pressure-gradient, *Journal of Fluid Mechanics* **21**, 173 (1965).
- [9] B. Joseph, E. P. Smith, and R. J. Adler, Numerical treatment of laminar flow in helically coiled tubes of square cross section. part i: Stationary helically coiled tubes, *AIChE Journal* **21**, 1045 (1975).
- [10] K. C. Cheng, R. Lin, and J. Ou, Fully developed laminar flow in curved rectangular channels, *Journal of Fluids Engineering* **98**, 41 (1976).
- [11] L. R. Austin and J. D. Seader, Fully developed viscous flow in coiled circular pipes, *AIChE Journal* **19**, 85 (1973).
- [12] R. J. Goldstein and D. K. Kreid, Measurement of laminar flow development in a square duct using a laser-doppler flowmeter, *ASME Journal of Applied Mechanics* **34**, 813 (1967).
- [13] K. N. Ghia and J. S. Sokhey, Laminar incompressible viscous flow in curved ducts of regular cross-sections, *ASME Journal of Fluids Engineering* **99**, 640 (1977).
- [14] J. A. C. Humphrey, A. M. K. Taylor, and J. H. Whitelaw, Laminar flow in a square duct of strong curvature, *Journal of Fluid Mechanics* **83**, 509 (1977).
- [15] S. A. Berger, L. Talbot, and L. S. Yao, Flow in curved pipes, *Annual Review of Fluid Mechanics* **15**, 461 (1983).
- [16] K. H. Winters, A bifurcation study of laminar flow in a curved tube of rectangular cross-section, *Journal of Fluid Mechanics* **180**, 343 (1987).

- [17] P. Daskopoulos and A. M. Lenhoff, Flow in curved ducts: bifurcation structure for stationary ducts, *Journal of Fluid Mechanics* **203**, 125 (1989).
- [18] H. C. Kao, Some aspects of bifurcation structure of laminar flow in curved ducts, *Journal of Fluid Mechanics* **243**, 519 (1992).
- [19] P. A. Mees, K. Nandakumar, and J. H. Masliyah, Instability and transitions of flow in a curved square duct: the development of two pairs of dean vortices, *Journal of Fluid Mechanics* **314**, 227 (1996).
- [20] H. Fellouah, C. Castelain, A. O. E. Moctar, and H. Peerhossaini, A criterion for detection of the onset of dean instability in newtonian fluids, *European Journal of Mechanics - B/Fluids* **25**, 505 (2006).
- [21] M. Kim and A. Borhan, Critical conditions for development of a second pair of dean vortices in curved microfluidic channels, *Physical Review E* **107**, 055103 (2023).
- [22] R. Macadré, F. Risso, O. Masbernat, and R. Belt, Primary and secondary motions in an annular plane couette flow, *Phys. Rev. F* **10**, 104102 (2025).
- [23] B. Harding and Y. Stokes, Fluid flow in a spiral microfluidic duct, *Phys. Fluids* **30** (2018).
- [24] Y. Saffar, S. Kashanj, D. S. Nobes, and R. Sabbagh, The physics and manipulation of dean vortices in single- and two-phase flow in curved microchannels: A review, *Micromachines* **14**, 2202 (2023).
- [25] I. Calmet and J. Magnaudet, Large-eddy simulation of high-schmidt number mass transfer in a turbulent channel flow, *Physics of Fluids* **9**, 438 (1997).
- [26] M. R. Jacques Magnaudet and J. Fabre, Accelerated flows past a rigid sphere or a spherical bubble. part 1. steady straining flow, *Journal of Fluid Mechanics* **284**, 97 (1995).
- [27] T. T. Chandratilleke, N. Nadim, and R. Narayanaswamy, Vortex structure-based analysis of laminar flow behaviour and thermal characteristics in curved ducts, *International Journal of Thermal Sciences* **59**, 75 (2012).
- [28] J. A. Baylis, Experiments on laminar flow in curved channels of square section, *Journal of Fluid Mechanics* **48**, 417 (1971).
- [29] A. Bottaro, On longitudinal vortices in curved channel flow, *J. Fluid Mech.* **251**, 627 (1993).
- [30] S. Sugiyama, T. Hayashi, and K. Yamazaki, Flow characteristics in the curved rectangular channels: Visualization of secondary flow, *Bulletin of JSME* **26**, 964 (1983).

- [31] N. Nivedita, P. Ligrani, and I. Papautsky, Dean flow dynamics in low-aspect ratio spiral microchannels, [Scientific Reports](#) **7**, 44072 (2017).
- [32] P. Bayat and P. Rezai, Semi-empirical estimation of dean flow velocity in curved microchannels, *Sci Rep.* **7**, 13655 (2017).
- [33] B. Harding, A new benchmark for the secondary fluid flow through curved ducts, *Chem. Eng. Sci.* **248**, 117196 (2022).
- [34] F. M. White, *Fluid Mechanics*, 7th ed. (McGraw-Hill, 2011).
- [35] L. Truesdell and R. Adler, Numerical treatment of fully developed laminar flow in helically coiled tubes, *AIChE J.* **16**, 1010 (1970).
- [36] T. Lin, *Laminar convective transport processes in strongly curved tubes* (Clarkson University, 1972).
- [37] O. J. E. Matsson and P. H. Alfredsson, Curvature- and rotation-induced instabilities in channel flow, [Journal of Fluid Mechanics](#) **210**, 537 (1990).



(a)



(b)

FIG. 9: Dimensionless radial pressure gradient  $\frac{1}{\delta} \frac{\partial \bar{P}}{\partial r}$  along the mid-plane  $\bar{x} = 0.5$  for (a) small Dean numbers and (b) moderate Dean numbers.

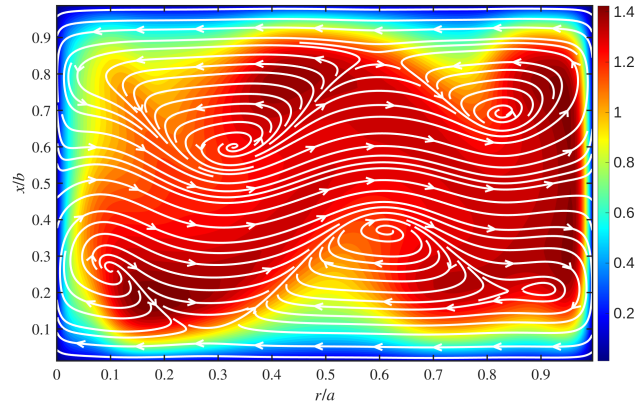


FIG. 10: Contours of the azimuthal velocity  $\bar{v}_\theta$  for  $De = 220$